DOI: 10.1002/chem.200800719

Hexa- and Dodecanuclear Polyoxomolybdate Cyclic Compounds: Application toward the Facile Synthesis of Nanoparticles and Film Electrodeposition

Anne Dolbecq,*[a] Jean-Daniel Compain,[a] Pierre Mialane,[a] Jérôme Marrot,[a] Francis Sécheresse,[a] Bineta Keita,[b] Luis Roberto Brudna Holzle,[b] Frédéric Miserque,[c] and Louis Nadjo*[b]

Abstract: Two new compounds based on $O_3PCH_2PO_3^{4-}$ ligands and $\{Mo^V_2O_4\}$ dimeric units have been synthesized and structurally characterized. The dodecanuclear Mo^V polyoxomolybdate species in $(NH_4)_{18}[(Mo^V_2O_4)_6(OH)_6(O_3PCH_2PO_3)_6]\cdot 33\,H_2O$ (**1**) is a cyclohexane-like ring in a chair conformation with pseudo S_6 symmetry. In the solid state, the wheels align side by side, thus delimiting large rectangular voids. The hexanuclear anion in $Na_8[(Mo^V_2O_4)_3(O_3PCH_2PO_3)_3(CH_3AsO_3)]\cdot 19\,H_2O$ (**2**) has a triangular framework and encapsulates a methylarsenato ligand. ^{31}P NMR spectroscopic analysis revealed the stability of **2** in various aqueous media, whereas the stability of **1** depends on the nature of the cations present in solution. It has been evidenced that the transformation of **1** into **2** occurs in the presence of $CH_3AsO_3^{2-}$ ions. This behavior shows that **1** can be used as a new precursor for the synthesis of Mo^V/diphosphonate systems. The two complexes were very efficient both as reductants of Pt and Pd metallic salts and as capping agents for the resulting Pt^0 and Pd^0 nanoparticles. The size of the obtained nanoparticles depends both on the nature of the polyoxometalate (POM; i.e., **1** or **2**) and on the [metallic salt]/[POM] ratio. In all cases, X-ray photoelectron spectroscopy (XPS) measurements have revealed the presence of Mo^{VI} species that stabilize the nanoparticles and the absence of Mo^V moieties. Diffuse-reflectance FTIR spectra of the Pt nanoparticles show that the capping Mo^{VI} POMs are identical for both systems and contain the diphosphonato ligand. The colloidal solutions do not show any precipitate and the nanoparticles remain well-dispersed for several months. The electrochemical reduction of Mo^V species was studied for **2**. Cyclic voltammetry alone and electrochemical quartz crystal microbalance coupled with cyclic voltammetry show the deposition of a film on the electrode surface during this reduction.

Keywords: electrochemistry · molybdenum · nanoparticles · NMR spectroscopy · polyoxometalates

[a] Dr. A. Dolbecq, J.-D. Compain, Dr. P. Mialane, Dr. J. Marrot, Prof. F. Sécheresse
Institut Lavoisier de Versailles, UMR 8180
Université de Versailles Saint-Quentin en Yvelines
45 Avenue des Etats-Unis, 78035 Versailles cedex (France)
Fax: (+33) 139-254-381
E-mail: dolbecq@chimie.uvsq.fr

[b] Dr. B. Keita, Dr. L. R. B. Holzle, Prof. L. Nadjo
Laboratoire de Chimie Physique
Groupe d'Electrochimie et de Photoélectrochimie
UMR 8000, CNRS, Université Paris-Sud
Bâtiment 350, 91405 Orsay cedex (France)
E-mail: nadjo@lcp.u-psud.fr

[c] Dr. F. Miserque
Laboratoire de Réactivité des Surfaces et Interfaces/CEA-Saclay
DEN/DANS/DPC/SCP
Bâtiment 391, 91191 Gif-sur-Yvette Cedex (France)

Supporting information for this article is available on the WWW under http://dx.doi.org/10.1002/chem.200800719.

Introduction

Organic derivatives of polyoxomolybdates are attracting increasing interest among the family of polyoxometalates (POMs). The stabilization and the design of original architectures and the modeling of catalytic or biological reactions are worthy of mention among the several goals hoped to be achieved by the incorporation of organic ligands into inorganic clusters.[1] Limiting this introduction to the polyoxomolybdate species in which the bridging oxo ligands are substituted by organic ligands, we may cite 1) the family of polyoxoalkoxometalates in which tris(alkoxo) ligands are incorporated into the POM framework,[2] 2) cyclic architectures[3] but also Keggin derivatives[4] obtained by the reaction of MoO_4^{2-} ions with organophosphonate and organoarsonate

ligands, and 3) heteropolymolybdates functionalized with amino acids[5] or phosphonocarboxylates.[6]

Besides these Mo^{VI} compounds, the chemistry of the $[Mo^{V}_2O_2S_2]^{2+}$ ion in aqueous solution has afforded a great diversity of cyclic oxothiomolybdates ions that encapsulate carboxylate ligands,[7] whereas only one analogous fully oxo Mo^{V} octanuclear wheel, built around an oxalate ligand, has been isolated in an organic medium.[8] Indeed, unlike the oxothiomolybdate rings, direct connections through bridging hydroxo ligands between the $\{Mo^{V}_2O_4\}$ building units have not been observed in aqueous solution. One way to circumvent this feature is to incorporate the organic $O_3PCH_2PO_3^{4-}$ ligand, which acts as a bridging ligand between the $\{Mo^{V}_2O_4\}$ building units, directly in the ring.

We have thus isolated eight different cyclic anions with the general formula $\{(Mo^{V}_2O_4)(O_3PCH_2PO_3)\}_n$ ($n=3$, 4, 10) that incorporate small organic or inorganic guests and have shown the crucial role of both the template and counterion in the structure of the cyclic anions.[9] One application of the electron-reservoir properties of these reduced molybdate anions has very recently been evidenced by the synthesis of Pd^0, Pt^0,[10] and Ag^0[11] nanoparticles. It has been shown that the polyoxomolybdate not only acts as a reductant but also stabilizes the nanoparticles. Furthermore, the size and shape of the nanoparticles depend on the POM used as the reductant. It is then essential to have a family of Mo^{V} compounds with various redox potentials to tune the characteristics of the nanoparticles.

We present herein the synthesis of two novel rings $\{(Mo^{V}_2O_4)(O_3PCH_2PO_3)\}_n$ ($n=3$, 6). The dodecanuclear wheel **1**, which does not contain any guest, adopts a particularly original cyclohexane-like topology. ^{31}P NMR spectroscopic studies have shown that this compound is metastable in aqueous solution and can be used as a precursor. Its reactivity in the presence of the methylarsenato ligand has been studied, thus leading to the isolation of the hexanuclear wheel **2**. The two complexes could be used for the synthesis of Pd and Pt nanoparticles and the results are described herein. Finally, a preliminary study of the reduction of Mo^{V} centers in **2** was undertaken by cyclic voltammetry and electrochemical quartz crystal microbalance coupled with cyclic voltammetry.

Results and Discussion

Synthesis and structure: In our previous studies,[9] the $[Mo_2O_4(H_2O)_6]^{2+}$ ion was obtained by reduction of an acidic solution of the molybdate precursor $[(NH_4)_6Mo^{VI}_7O_{24}]$, $[Na_2Mo^{VI}O_4]$, or $[Li_2Mo^{VI}O_4]$ with hydrazine, and the pH value was raised with NH_3, NaOH, or LiOH respectively. We modified our synthetic protocol to have a single starting solution of Mo^{V} ions that does not contain any alkaline or ammonium cations. This solution is obtained by the reduction of a suspension of MoO_3 in 4 M HCl with hydrazine. The desired countercation can then be introduced by raising the pH value either with NH_3, NaOH, or LiOH. The new dodecanuclear wheel $[(Mo^{V}_2O_4)_6(OH)_6(O_3PCH_2PO_3)_6]^{18-}$ in **1** has thus been isolated, with $O_3PCH_2PO_3^{4-}$ as the only ligand and ammonium counterions, together with the hexanuclear $[(Mo^{V}_2O_4)_3(O_3PCH_2PO_3)_3(CH_3AsO_3)]^{8-}$ ion, with a central methylarsonato ligand and sodium counterions, in **2** (Scheme 1).

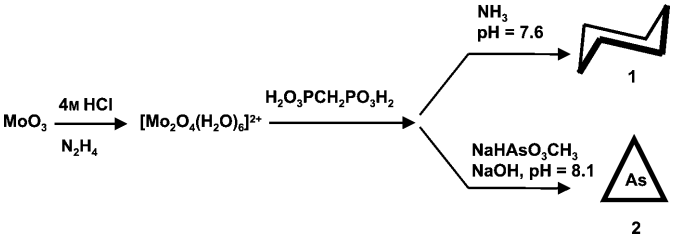

Scheme 1. Synthetic routes to **1** and **2**.

As previously observed in this family of compounds, $\{(Mo_2O_4)(O_3PCH_2PO_3)\}$ is the structural building unit in **1** and **2**. In this structural unit, one of the two edge-sharing Mo^{V} octahedra (in which the Mo^{V} ions are connected by a metal–metal bond of around 2.6 Å) is linked to the two P–O groups of the bistetrahedral organophosphonato ligand (Figure 1a). In **1**, six of these units alternate and form the

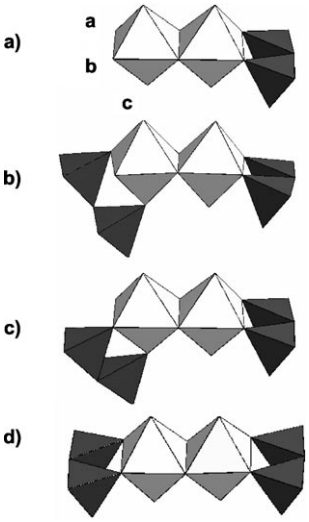

Figure 1. Structure of the $\{(Mo^{V}_2O_4)(O_3PCH_2PO_3)\}$ unit. a–c) Three possible positions for the anchoring of the methylenephosphonato ligand; white octahedra: MoO_6, dark gray tetrahedra: PO_3C.

cyclohexane-like ring $[(Mo^{V}_2O_4)_6(OH)_6(O_3PCH_2PO_3)_6]^{18-}$ in a chair conformation in which the methylenediphosphonato ligands are at the vertices and the edge-sharing Mo^{V} octahedra are at the edges (Figure 2b). The $\{(Mo_2O_4)(O_3PCH_2PO_3)\}$ structural units are connected through the a and c positions (Figure 1b) of the Mo^{V} octahedron and b and c positions (Figure 1c) alternatively. This feature is unusual as the connections are symmetrical on each side of the Mo^{V} dimer in all the hexa- and octanuclear

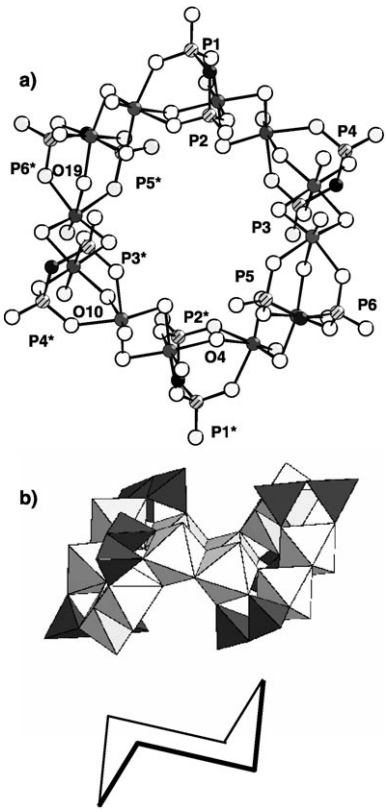

Figure 2. a) Ball-and-stick representation of the anion in **1**; dark gray sphere: Mo; white sphere: O; hatched light gray sphere: P; black sphere: C. b) Side view of the polyhedral representation of the anion in **1**, thus showing the analogy with the chair conformation of cyclohexane; white octahedra: MoO_6, dark gray tetrahedra: PO_3C.

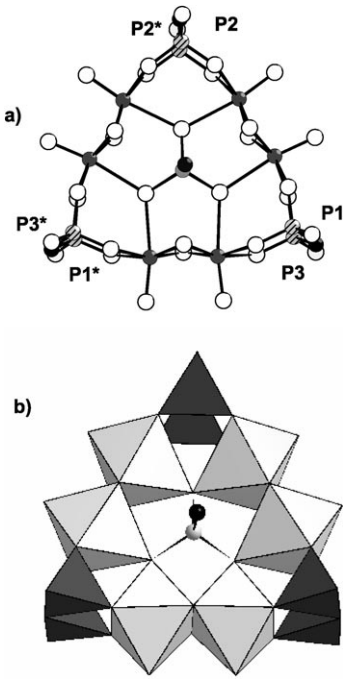

Figure 3. Ball-and-stick representation of the anion in **2**; dark gray sphere: Mo; white sphere: O; hatched light gray sphere: P; black sphere: C; medium gray sphere: As. b) Polyhedral representation of the anion in **2**; white octahedra: MoO_6; dark gray tetrahedra: PO_3C.

wheels of this family (i.e., at the a and b positions; Figure 1d).[9] The Mo^V dimers share one corner with the adjacent dimer. The bond lengths between the Mo^V ions and the oxygen atom that bridges two $\{(Mo_2O_4)(O_3PCH_2PO_3)\}$ subunits are long (Mo–O = 2.065(6)–2.238(6) Å), thus indicating that this oxygen atom is protonated, as confirmed by bond-valence calculations[12] ($\Sigma s(O18) = 1.08$, $\Sigma s(O10) = 1.08$, $\Sigma s(O4) = 1.11$). In the crystallographically determined structure, the dodecanuclear wheel exhibits only one symmetry element, that is, an inversion center, but pseudo C_3 and S_6 axes can be identified so that the wheel has pseudo S_6 symmetry. In the solid state, the wheels align side by side along the *c* axis, thus delimiting large rectangular voids filled by disordered water molecules and ammonium counterions (see Figure SI1 in the Supporting Information).

The anion in **2** possesses three $\{(Mo_2O_4)(O_3PCH_2PO_3)\}$ structural building units. The Mo^V edge-sharing octahedra are symmetrically connected at the a and b positions (Figure 1d), thus forming a triangle that encapsulates the $CH_3AsO_3^{2-}$ ligand (Figure 3). In the crystal structure, the anion lies on a C_2 axis that passes through the carbon atom bound to P2 and P2* and the middle of the Mo–Mo bond of the Mo^V dimeric unit on the opposite edge. It follows that the arsenic atom of the methylarsenato ligand, which is located 0.58 Å above the $\{Mo_6\}$ plane, is disordered over two positions related by the C_2 axis. The triangular architecture is reminiscent of that of the hexanuclear wheel $[(Mo^V_2O_4)_3(O_3PCH_2PO_3)_3(Mo^{VI}O_4)]^{8-}$, with one tetrahedral Mo^{VI} ion in the center of the triangle.[9] Two hexanuclear polyoxomolybdate ions with methylarsenato ligands have been previously characterized, namely, the $[Mo_6O_{18}(CH_3AsO_3)(H_2O)_6]^{2-}$[13] and $[Mo_6O_{18}(CH_3AsO_3)_2]^{4-}$ complexes,[14] but this structure is the first in which the $CH_3AsO_3^{2-}$ ion has been incorporated into a reduced polyoxomolybdate anion. Note also that hexanuclear Mo^{VI}[15] and dodecanuclear W^{VI}[16] POMs with methylenediphosphonate ligands have already been reported, but their composition and topologies are quite different from that of **1** and **2**.

^{31}P NMR spectroscopic studies: As reported previously,[9] ^{31}P NMR spectroscopy is a powerful tool with which to investigate the stability of the organophosphonates polyoxomolybdate compounds and demonstrate possible dynamic equilibrium in solution. Thus, ^{31}P NMR spectroscopic studies have shown that the dodecanuclear wheel in **1** degrades rapidly into unknown products in pure water, 1 M LiCl, and 1 M NH_4Cl but is stable for at least 15 min in 1 M NaCl at room temperature (Figure 4). This behavior once again highlights the crucial role played by the countercations in the stability of these highly charged cyclic Mo^V systems.[9b] The influence of the countercations on the formation and the stability of Mo^{VI}[17] and W^{VI}[18,19] POMs has also already been shown. The ^{31}P NMR spectrum of a fresh solution of **1** in 1 M NaCl

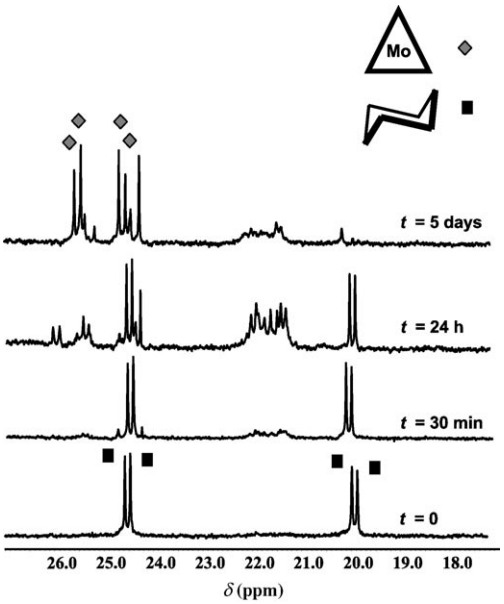

Figure 4. Evolution of the ^{31}P NMR spectrum of a solution of **1** with time in 1 M NaCl ($[\mathbf{1}]=9.3\times10^{-3}$ mol L^{-1}).

exhibits a doublet of doublets, thus indicating that the six methylenediphosphonato ligands are equivalent in solution, as expected considering the S_6 symmetry of the dodecanuclear wheel; that is, one doublet is attributed to the six equivalent P1, P4, P6, P1*, P4*, and P6* atoms (Figure 2a) and the other doublet to the remaining six equivalent P2, P3, P5, P2*, P3*, and P5* atoms. The coupling constant ^2J(P-C-P) = 13.7 Hz between P1 and P2, deduced from the ^{31}P NMR spectrum, is close to the one observed for other methylenediphosphonate/POM systems.[9] After 30 min, several extra peaks appear that show the slow decomposition of **1**. The peaks of the initial compound **1** and some of the intermediate species progressively disappear with time. The peaks of the majority species observed after five days are attributed to the previously characterized hexanuclear $[(Mo^{V}_2O_4)_3(O_3PCH_2PO_3)_3(Mo^{VI}O_4)]^{8-}$ ion (marked with diamonds on Figure 4).[9] These species must result from the decomposition of the dodecanuclear wheel, its partial oxidation in air, and its rearrangement around a central tetrahedral $\{Mo^{VI}O_4\}$ core.

The hexanuclear wheel in **2** is stable at room temperature in aqueous solution (pure water, 1 M LiCl, 1 M NaCl, and 1 M NH_4Cl) over a period of several days. The ^{31}P NMR spectrum of **2** exhibits a doublet of doublets at $\delta=25.55$, 25.42, 23.52, and 23.39 ppm (^2J(P-C-P) = 15.6 Hz) attributed to the three equivalent P1, P2, and P3 atoms, coupled with the three equivalent P1*, P2*, and P3* atoms (Figure 5a top). We studied the evolution of the ^{31}P NMR spectrum of a solution of **1** in 1 M NaCl in the presence of $CH_3AsO_3H^-$ ions (Figure 5). The relative intensity of the doublet of doublets attributed to **1** (marked with black squares) progressively decreases while several resonances appear. A comparison with the ^{31}P NMR spectrum of **2** clearly shows that **1** evolves into **2** (peaks marked with black circles). After 2 h, the resonances attributed to **1** have completely disappeared. A doublet of doublets of an unknown species at $\delta=21.9$, 21.8, 21.3, and 21.2 ppm (black triangles) appear concomitantly with the resonances of **2**, but its relative intensity progressively decreases and thus can be attributed to an intermediate species. On the other hand, several small resonances appear around $\delta=21.5$ ppm and their intensities do not change after 2 h, thus indicating that a minority secondary product is also formed. Figure 5b shows a quantitative analysis of the evolution of **1**, **2**, and the unidentified intermediate species.

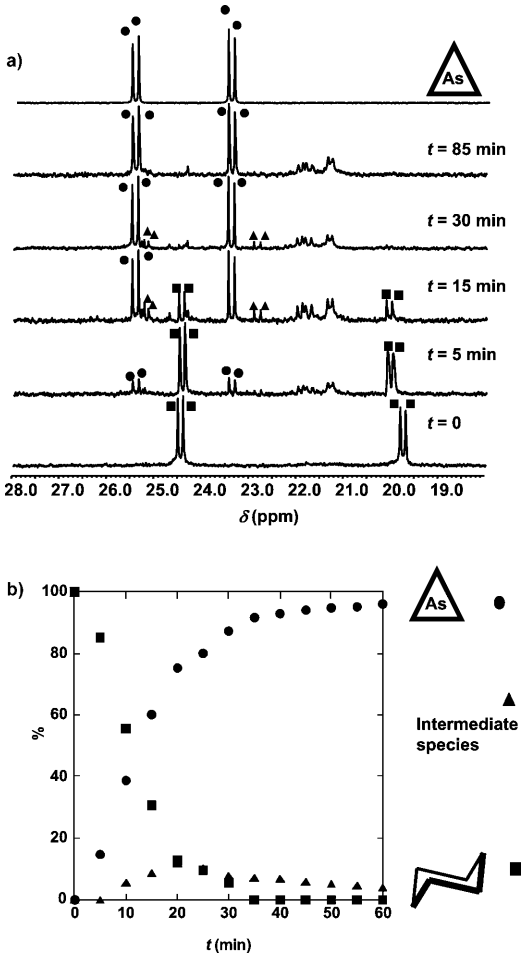

Figure 5. a) ^{31}P NMR spectrum of a solution of **2** in 1 M NaCl ($[\mathbf{2}]=1.7\times10^{-2}$ mol L^{-1}) (top) and changes in the ^{31}P NMR spectrum of **1** dissolved in a solution of $CH_3AsO_3H^-$ ions in 1 M NaCl ($[\mathbf{1}]=9.3\times10^{-3}$ mol L^{-1}; $[CH_3AsO_3H^-]/[\mathbf{1}]=4{:}1$). b) Evolution of the proportion of **1** and **2** deduced by the integration of the peaks.

The ^{31}P NMR spectroscopic studies have therefore shown that **2** is stable in aqueous solution in the presence of various counterions and that **1** evolves into **2** in the presence of methylarsonato ligands and into the triangular $[(Mo^{V}_2O_4)_3(O_3PCH_2PO_3)_3(Mo^{VI}O_4)]^{8-}$ species in air (Scheme 2).

Synthesis of Pd and Pt nanoparticles with 1 or 2 as reductants: Recent studies from our groups have demonstrated

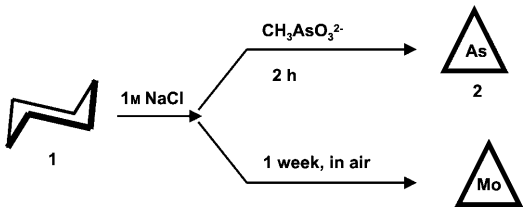

Scheme 2. Synthetic routes to **2** from the precursor **1**.

that selected POMs are potentially good candidates for the synthesis of various metallic nanoparticles under mild conditions.[10,11,20] With the present compounds, it is anticipated that the presence of Mo^V species in the building blocks of **1** and **2** and the measured formal potential of the Mo^{VI}/Mo^V redox couple within these complexes (−0.150 V versus the saturated calomel electrode (SCE) and +0.030 V versus SCE for **1** and **2**, respectively, in a medium of pH 2 (1 M LiCl + HCl) constitute favorable conditions for the synthesis of metallic nanoparticles.

The syntheses of Pd and Pt nanoparticles in aqueous media from $PdCl_4^{2-}$ and Pt^{2+} moieties are described by using the following as test examples: The corresponding formal potentials for $Pd^0/PdCl_4^{2-}$ and Pt^0/Pt^{2+} are +0.350 and +0.876 V versus SCE, respectively. In a typical experiment, a mixture containing 0.5 mM POM (unless otherwise stated) and variable concentrations of the appropriate metallic salt was assembled in water. The excess parameter is defined as γ = [metallic salt]/[POM] and was optimized for each synthesis. The mixture was kept at room temperature throughout. After mixing the POMs with $PdCl_4^{2-}$ or Pt^{2+} species, the solution gradually changed from orange to the characteristic brown color of Pd^0 nanoparticles or to the black color of Pt^0 nanoparticles. Actually, the UV/Vis spectrum of the mixture evolved from the POM and was gradually dominated by the intense, but featureless, surface plasmon resonance band (SPR) that is indicative of the formation of nanoparticles.

For clarity, the main observations will be described for **1** and compared briefly with those obtained with **2**. Complementary details for **2** are given in the Supporting Information. Figure 6 shows a representative transmission electron microscopy (TEM) image of Pd^0 nanoparticles synthesized with **1** by using an excess parameter of 2. This sample was centrifuged and washed several times. The X-ray photoelectron spectroscopy (XPS) analysis confirms that Pd^0 nanoparticles constitute the majority of the Pd species deposited on the analysis grid (Figure 7). Note that no particular care was

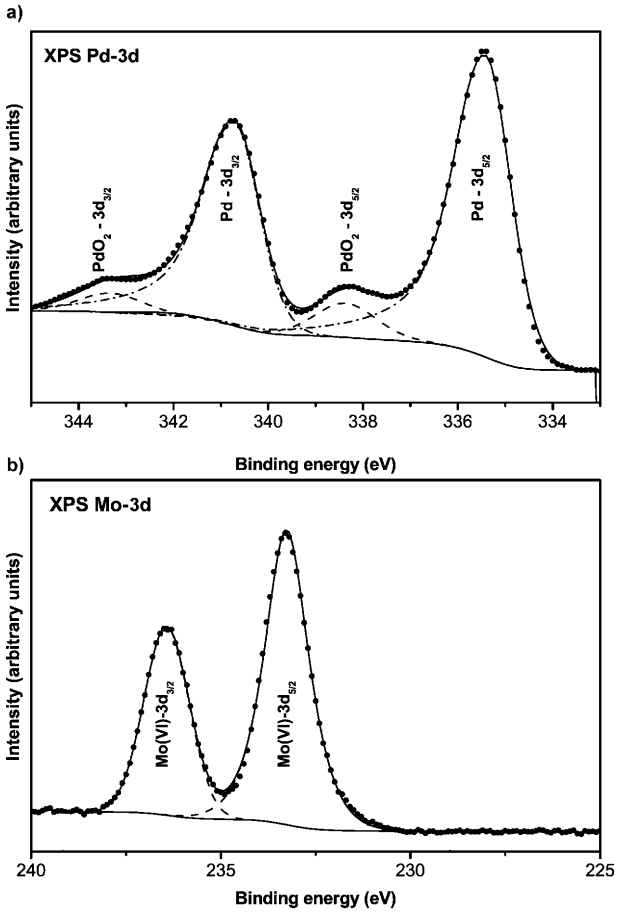

Figure 7. a) Deconvolution of the XPS spectrum of the Pd core 3d levels. The synthesis was carried out with **1** as the reductant, the mixture was centrifuged and washed before deposition. Two oxidation states were detected for Pd: Pd^0 (located at 335.0 ± 0.3 and 340.6 ± 0.3 eV, respectively, for the $3d_{5/2}$ et $3d_{3/2}$ levels) and Pd^{IV} (338.4 ± 0.3 and 343.5 ± 0.3 eV, respectively, for the $3d_{5/2}$ and $3d_{3/2}$ levels). Pd^0 is the more abundant species in the mixture (see the text for further details). b) Deconvolution of the XPS spectrum of the Mo core 3d levels: only Mo^{VI} was detected.

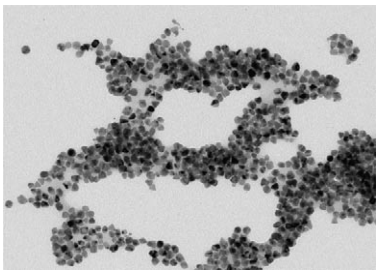

Figure 6. TEM image of Pd^0 nanoparticles synthesized with **1** as a reducing agent using an excess parameter γ of 2 (see the text for further details).

exercised to avoid any possible oxidation of the solution during the handling steps. A detail deserving emphasis is the presence of Mo^{VI} species in spite of washing, an indication that the nanoparticles are associated with the oxidized POM. Taking into account the Scofield sensitivity factors, the relative atomic composition of the analyzed deposit is 57% Mo and 43% Pd. In agreement with previous studies, the POM appears to serve both as the reductant of the metallic salt and the capping agent of the resulting nanoparticles.[10,11,18]

The nanocrystallites observed in Figure 6 exhibit a relatively narrow size distribution (average: 9–14 nm). Replica-

tion of the same experiment with $\gamma=2$ and 0.2 mM POM (instead of 0.5 mM POM) shows no significant variation in the size distribution (8–16 nm). In contrast, the combination of $\gamma=1$ with 0.5 mM POM gives a larger dispersity (7–41 nm). Slightly larger faceted particles that showed a narrow distribution also (24–30 nm for $\gamma=1$ and 0.5 mM POM) were observed for Pd^0 nanoparticles synthesized with **2** (see Figure SI2 in the Supporting Information). Taking into account the Scofield sensitivity factors in the XPS analysis (see Figure SI3 in the Supporting Information), the relative atomic composition of the analyzed deposit is 4% Mo and 96% Pd. Upon varying γ from 0.5 to 4 with this last POM, we found that the excess parameter markedly influences the size distribution (see Table SI1 in the Supporting Information). The presence of Mo was also detected, as expected.

In short, the size and compositional distributions are heavily dependent on the ability of POMs to adsorb on metal surfaces. It is also noteworthy that the known considerations refer essentially to bulk metal surfaces. This adsorption strength depends both on the metal, the POM, and the redox state of the POM. It should also be noted that the reduction affects the ability of POMs to be sorbed on metal surfaces, which decreases in some cases[21] and increases in others.[22] Previous reports[23] and our own studies[11] show that the excess parameter and the overall reaction kinetics, including the competition of the oxidized and reduced forms of the original reductant for adsorption on the synthesized nanoparticles, are also parameters that govern the size and morphology of the synthesized nano-objects (i.e., spherical nanoparticles, nanowires, and so forth).

The synthesis of Pt^0 both by **1** or **2** yields very small nanoparticles. Figure SI4 in the Supporting Information shows a TEM image of the remarkably monodisperse Pt^0 nanoparticles obtained by using **1** as the reductant with several γ values. In this synthesis, the excess parameter γ was 10, and 0.5 mM POM was used. The size distribution was 1.7–2 nm. A slight variation in γ value from 10 to 9 does not significantly modify this size distribution (2.5–3 nm). XPS analysis of the mixture obtained with $\gamma=4$ (see Figure SI5 in the Supporting Information) confirms the presence of Pt^0, associated with an excess of Pt^{II}. Concerning Mo ions, only Mo^{VI} was detected, the presence of which in spite of the washing, indicates that the nanoparticles are associated with the oxidized POM. Taking into account the Scofield sensitivity factors, the relative atomic composition of the analyzed deposit is 27% Mo and 73% Pt. The formation of crystallized Pt^0 nanoparticles was confirmed by powder X-ray diffraction (see Figure SI6 in the Supporting Information). All X-ray diffraction peaks could be assigned to face-centered cubic Pt. The presence of an excess of Pt^{II} ions and of exclusively Mo^{VI} species in the XPS analysis suggests the following considerations. First, the use of an excess parameter γ of 4 in this experiment guarantees that there is more than the theoretically necessary amount of reductant to reduce all the Pt ions in the starting solution. Second, monitoring with UV/Vis spectroscopy of the mother solution used for the preparation of the XPS samples over several days and the XPS analysis confirm the complete consumption of **1** during the process of nanoparticle synthesis. As a consequence, it can be proposed that a complicated nonpurely redox Pt^0 etching mechanism should exist in this system. Another possibility could be the presence of an amorphous Pt^{II} salt of the oxidized form of the POM precipitating concomitantly to the formation of Pt^0 nanoparticles, as already observed for Ag nanoparticles stabilized by $[H_5PV_2Mo_{10}O_{40}]$.[24] Two representative TEM images captured from two areas of the analysis grid for Pt^0 nanoparticles synthesized by **2** are shown in Figure 8 for $\gamma=4$ and 0.5 mM POM. The synthesis of Pt^0 nanoparticles was confirmed by powder X-ray diffraction and XPS studies (see Figure SI6 and Figure SI7, respectively, in the Supporting Information), which also indicate a relative atomic composition of 13% Mo and 87% Pt in the deposit, when taking into account the Scofield sensitivity factors.

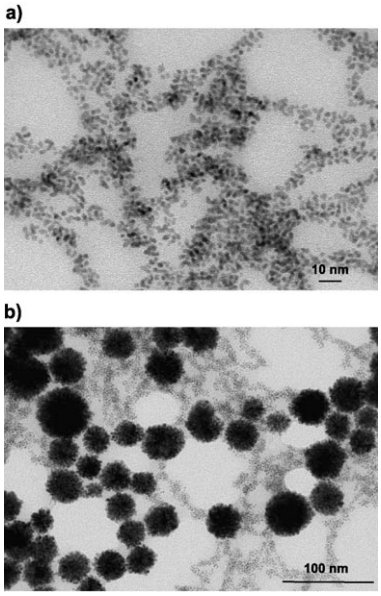

Figure 8. a) TEM image of Pt^0 nanoparticles synthesized with **2** as the reducing agent with $\gamma=4$ (see the text for further details). b) TEM image of Pt^0 nanoparticles synthesized with **2** as the reducing agent with $\gamma=4$, thus showing the gradual formation of urchin-like structures (see the text for further details).

The crystallites in Figure 8a are quasi-monodisperse and their sizes vary from 1.8 to 3 nm. Relative to Figure SI4 in the Supporting Information, this image does not call for further comment. In contrast, Figure 8b displays an area in which quasi-monodisperse large aggregates appear. The image is interesting because it suggests a gradual coalescence mechanism by which small-size nanoparticles aggregate to build up large crystallites. We wondered whether centrifugation and washing could induce or favor such aggregation. Actually, detailed exploration of the deposit directly from the mother solution on a TEM grid revealed that a limited number of such urchin-like structures exist

prior to centrifugation and washing. It is remarkable that all the aforementioned nanoparticles remain well-dispersed in solution for months. The formation of urchin-like structures could be of interest in the field of catalysis, as it has already been shown that the catalytic performances of metallic nanoparticles are highly dependent on the shape of the particles.[25]

We performed FTIR spectroscopic analysis of the POMs-protected Pt nanoparticles to better characterize the nature of the Mo^{VI} POMs at the surface of the nanoparticles. The colloidal solution containing the nanoparticles was left to evaporate on glass slides. A comparison of the FTIR spectra of pure **1** and **2** solids deposited on glass sides and of Pt nanoparticles obtained from the reaction of **1** and **2** with Pt^{IV} ions (see Figure SI8 in the Supporting Information) confirms that the POMs adsorbed at the surface are not the initial Mo^{V} POMs and that their structure is similar for both nanoparticles. Furthermore, Mo–O (around $\tilde{\nu}=950\,cm^{-1}$) and P–O (around $\tilde{\nu}=1010$ and $1160\,cm^{-1}$) stretching bands are clearly identified on the spectra, thus indicating that a Mo^{VI}/methylenediphosphonate POM is attached to the nanoparticles. The structure of this POM is different from that of the $[(O_3PCH_2PO_3)Mo_6O_{18}(H_2O)_4]^{4-}$ ion,[15] as indicated by significant differences in their IR spectra. Unfortunately, the spectra recorded for the Pd nanoparticles were not of sufficiently good quality so no complementary information can be given concerning the nature of the Mo^{VI} POMs deposited at the surface of the Pd nanoparticles.

Reduction processes of Mo^{V} centers: The Mo^{V} centers of the present POMs are also reducible. Curve 1 in Figure 9 shows the very first voltammogram registered in a solution of **2** in a solution at pH 2 (1 M LiCl + HCl) between −0.150 and −1.200 V. This peak, which features the reduction of Mo^{V} centers, is located around −1.150 V and is followed by the proton-discharge wave (not shown in Figure 9). On potential reversal, a well-defined oxidation wave that peaked at −0.370 V is associated with the Mo reduction wave. From the second voltammetric run, an important positive potential shift of 0.450 V is observed for the cathodic wave, whereas the potential location of the oxidation wave remains practically constant. On subsequent runs, only a slight positive potential shift of the cathodic peak is observed, whereas both the reduction and oxidation currents increase. Concomitantly, the oxidation wave becomes composite. The current increase after every other run probably indicates a film growth on the electrode surface. A simultaneous and large improvement of the reversibility of the redox processes is noted and is revealed by a more symmetrical shape of the voltammetric pattern. For example, an anodic-to-cathodic peak potential difference $\Delta E=0.780$ V is measured for the very first voltammogram, but decreases to 0.330 V for the second run.

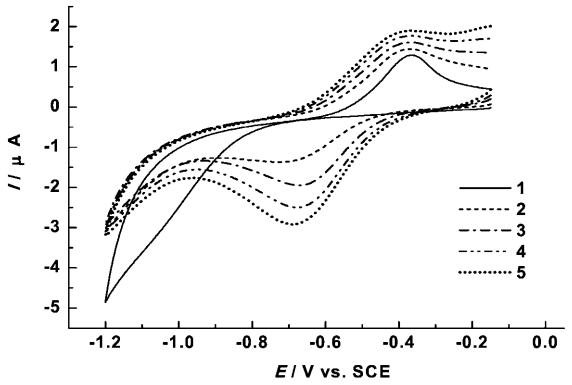

Figure 9. Evolution of the cyclic voltammogram of 2×10^{-4} M of **2** in a solution at pH 2 (1 M LiCl+HCl) as a function of the number of runs. The scan rate was $10\,mV\,s^{-1}$, the working electrode was a glassy carbon disk, and the reference electrode was SCE (see the text for further details).

The following mechanism can explain such an improvement in the wave characteristics with the number of runs: The first film layer deposited on the electrode might contain a paucity of electrolyte and therefore should be compact and poorly conductive, possibly under a molecular form; subsequent layers should be more porous salt forms, with a high electrolyte-uptake capacity, thus favoring electron-transfer processes. However, it must be noted that very thick films show more complex characteristics; in particular, an ohmic drop results, as expected, into a slight shift of the cathodic peak in the negative potential direction and a slight shift of the anodic peak in the positive direction. Analogous behavior was observed previously during the deposition of films obtained with reduced products from POMs, such as $[P_2Mo_{18}O_{62}]^{6-}$ and $[(HOAs)_4Mo_{12}O_{46}]^{4-}$ ions by potential cycling and the potentiostatic method.[26,27] It must be noted that in both cases, the necessary number of electrons for film formation is larger than 6. Further confirmation of such film deposition was obtained by coupling electrochemical quartz crystal microbalance with cyclic voltammetry (see the Supporting Information).

Conclusion

In conclusion, the acid/base condensation of the $[Mo^{V}_2O_4(H_2O)_6]^{2+}$ oxo ion with $O_3PCH_2PO_3^{4-}$ ligands has afforded two novel cyclic species. The dodecanuclear $[(Mo^{V}_2O_4)_6(OH)_6(O_3PCH_2PO_3)_6]^{18-}$ ion can be described as a cyclohexane-like ring in a chair conformation, a unique feature in this family of otherwise planar cyclic compounds. The hexanuclear $[(Mo^{V}_2O_4)_3(O_3PCH_2PO_3)_3(CH_3AsO_3)]^{8-}$ ion has a triangular shape and encapsulates a $CH_3AsO_3^{2-}$ group, which opens the way to the functionalizaton of the wheel by the introduction of more sophisticated organoarsenato groups. Furthermore, ^{31}P NMR spectroscopic studies have shown that the dodecanuclear anion can react at pH $\approx$8 with the methylarsenato ligand to quantitatively give the hexanuclear anion. This behavior demonstrates that the $[(Mo^{V}_2O_4)_6(OH)_6(O_3PCH_2PO_3)_6]^{18-}$ ion can be used as a precursor for the synthesis of new Mo^{V} wheels at neutral pH in contrast with the previously reported synthesis in which the $[Mo^{V}_2O_4(H_2O)_6]^{2+}$ ion in 4 M HCl was considered.

Ligands sensitive to acidic conditions could then be used. The two complexes proved useful for the efficient synthesis of Pt and Pd nanoparticles, which remain perfectly stable in solution.

These results add a new illustration to the polyoxometalate-based mild synthesis of metallic nanoparticles in water at room temperature pioneered by our groups. It is expected that accumulation and detailed analysis of such examples will help to establish correlation guides for the choice of POMs and associated morphologies of resulting metallic nanoparticles.

Electrochemically deposited films have also been obtained from the reduction of the hexanuclear POM presented herein. It remains to be shown that these electrodeposited films can be prepared with other functionalized Mo^{V} POMs. Moreover, such materials are expected to show interesting electrocatalytic behavior. Corresponding studies will be described in future studies.

Experimental Section

Preparation of a 0.10 M solution of $[Mo_2O_4(H_2O)_6]^{2+}$ ions in 4 M HCl: $N_2H_4{\cdot}H_2O$ (210 μL, 4.29 mmol) was added to a suspension of MoO_3 (2.30 g, 16 mmol) in 4 M HCl (80 mL). The solution turned progressively to red while stirring for 3 h at 60 °C.

Synthesis of $(NH_4)_{18}[(Mo^{V}_2O_4)_6(OH)_6(O_3PCH_2PO_3)_6]{\cdot}33H_2O$ (1): $H_4P_2CH_2O_6$ (0.227 g, 1.29 mmol) was dissolved in a solution of $[Mo_2O_4(H_2O)_6]^{2+}$ (12.9 mL, 1.29 mmol) obtained from the reduction of MoO_3 as described above and the pH value was increased to pH 7.6 by the dropwise addition of 33% NH_3 solution. The solution was then left to evaporate at room temperature. Red parallelepipedic crystals were collected by filtration after one week (0.51 g, 78% based on Mo). FTIR (KBr pellets): $\tilde{\nu}$ = 1444 (m, sh), 1398 (s), 1171 (s), 1141 (m), 1101 (m), 1053 (s), 1019 (s), 950 (sh), 924 (s), 791 (w), 744 (w), 528 (w), 470 (w) cm^{-1}; elemental analysis (%) calcd for $C_6H_{156}Mo_{12}N_{18}O_{99}P_{12}$ (3588.35): C 2.00, H 4.38, N 7.03, Mo 32.08, P 10.36; found: C 2.16, H 4.09, N 7.45, Mo 31.24, P 10.10.

Synthesis of $Na_8[(Mo^{V}_2O_4)_3(O_3PCH_2PO_3)_3(CH_3AsO_3)]{\cdot}19H_2O$ (2): A solution of $[Mo_2O_4(H_2O)_6]^{2+}$ (12.9 mL, 1.29 mmol) was obtained from the reduction of MoO_3 as described above, and the pH value was increased to pH 1.2 by the dropwise addition of 8 M NaOH. $Na[CH_3AsO_3H]$ (0.112 g, 0.69 mmol) was dissolved in the $[Mo_2O_4(H_2O)_6]^{2+}$ solution. $H_4P_2CH_2O_6$ (0.227 g, 1.29 mmol) was then added and the pH value was increased to pH 8.1 by the dropwise addition of 8 M NaOH. The solution was then left to evaporate at room temperature. After 1 week, red parallelepipedic crystals were collected by filtration (0.29 g, 54% based on Mo). FTIR (KBr pellets): $\tilde{\nu}$ = 1188 (m), 1155 (s), 1118 (w), 1069 (s), 1030 (s), 975 (sh), 950 (s), 885 (w), 803 (m), 772 (w), 742 (m), 561 (w), 508 (m), 453 (m), 340 (m) cm^{-1}; elemental analysis (%) calcd for $C_4H_{47}AsMo_6Na_8O_{52}P_6$ (1947.71): C 2.47, As 3.85, Mo 29.55, Na 9.44, P 9.54; found: C 2.48, As 3.92, Mo 29.69, Na 8.93, P 9.45.

X-ray crystallographic studies: Intensity-data collections were carried out with a Siemens SMART three-circle diffractometer equipped with a CCD bidimensional detector using the monochromatized wavelength $\lambda(Mo_{K\alpha})$ = 0.71073 Å. The absorption correction was based on multiple and symmetry-equivalent reflections in the data set using the SADABS program[28] based on the method of Blessing.[29] The structures were solved by direct methods and refined by full-matrix least-squares using the SHELX-TL package.[30] In the structures of **1** and **2**, there is a discrepancy between the formulae determined by elemental analysis and the formulae deduced from the crystallographic atom list because of the difficulty in locating all the disordered water molecules and alkali counterions. In the structures of **1**, NH_4^+ and H_2O could not be distinguished according to the observed electron densities; therefore, all the positions were labeled O and assigned the oxygen atomic diffusion factor. Crystallographic data are given in Table 1.

Table 1. Crystallographic data for **1** and **2**.

	1	**2**
empirical formula	$C_6H_{156}Mo_{12}N_{18}O_{99}P_{12}$	$C_4H_{47}AsMo_6Na_8O_{51}P_6$
formula weight [g]	3588.40	1931.72
crystal system	monoclinic	monoclinic
space group	*C2/c*	*C2/c*
a [Å]	31.261(10)	21.290(3)
b [Å]	20.831(10)	21.441(3)
c [Å]	18.186(7)	13.538(3)
β [°]	113.387(11)	125.26(2)
V [Å^3]	10870(8)	5046(1)
Z	4	4
ρ_{calcd} [g cm^{-3}]	2.193	2.543
μ [mm^{-1}]	1.643	2.484
data/parameters	15751/586	6590/359
R_{int}	0.0646	0.0541
GOF	0.997	1.130
$R(>2\sigma(I))$	R_1[a] = 0.0624, wR_2[b] = 0.1754	R_1 = 0.0415, wR_2 = 0.1227

[a] $R_1 = \frac{\sum_{||F_0|-|F_c||}}{\sum |F_c|}$. [b] $wR_2 = \sqrt{\frac{\sum w(F_0^2-F_c^2)^2}{\sum w(F_0^2)^2}}$.

CCDC-684815 (**1**) and CCDC-684816 (**2**) contain the supplementary crystallographic data for this paper. These data can be obtained free of charge from The Cambridge Crystallographic Data Centre via www.ccdc.cam.ac.uk/data_request/cif

NMR spectroscopic measurements: The ^{31}P NMR spectra were recorded on a Brüker AC-300 spectrometer operating at 121.5 MHz in 5-mm tubes with ^1H decoupling. ^{31}P NMR chemical shifts were referenced to the external usual standard 85% H_3PO_4. For the ^{31}P NMR spectroscopic study shown in Figure 5, **1** (20 mg, 5.57×10^{-6} mol) was added to a $Na[AsCH_3O_3H]$ solution (600 μL, 0.046 M) adjusted to pH 8.3.

Elemental analysis: The elemental analyses were performed by the Service Central d'Analyse Elémentaire, CNRS, 69390 Vernaison France.

FTIR spectroscopic analysis: The IR spectra of complexes **1** and **2** were recorded on an IRFT Magna 550 Nicolet spectrophotometer by using the technique of pressed KBr pellets. Diffuse-reflectance FTIR (DRIFT) of the Pt nanoparticles were recorded on a Brüker IFS 66 V spectrometer with an ATR module with a diamond crystal from Pike Technologies in the range 4000–700 cm^{-1} (resolution: 2 cm^{-1}, 64 scans per spectrum). A few droplets of the colloidal solution were deposited on a glass slide and left to evaporate before recording the spectra.

Synthesis of Pd and Pt nanoparticles: K_2PtCl_4 and K_2PdCl_4 were selected as the metallic precursors. The platinum salt was dissolved in high-purity Millipore water (18 MΩ cm) and aged for 48 h prior to initiation of the reduction reaction, which allows the complex to aquate. In a typical experiment, a mixture containing 0.5 mM POM (unless otherwise stated) and variable concentrations of the appropriate metallic salt was assembled in water. The excess parameter is defined as γ = [metallic salt]/[POM] and was optimized for each synthesis. The reaction mixture was kept at room temperature throughout. Following the mixing of the POMs with $PdCl_4^{2-}$ or Pt^{2+} ions, the solution gradually changed from orange to the characteristic brown color of Pd^0 nanoparticles or to the characteristic black color of Pt^0 nanoparticles over a period of 24 h. The solution was centrifuged and the supernatant solution was replaced by water. This procedure was repeated four times. The size distribution of the Pd nanoparticles observed as a function of the excess parameter and the initial POM concentration are given in the text for **1** and reported in Table SI1 (see the Supporting Information) for **2**.

XPS characterization of Pd and Pt nanoparticles: The samples for XPS analysis were deposited on silicon wafers as supports. The XPS spectrometer was a Thermo Electron ESCALAB 220i XL. A non-monochromatic X-ray $Al_{K\alpha}$ source was used for excitation with an incident energy of 1486.6 eV. The X-ray power was 300 W (20 mA × 15 kV). The pass energy was 20 eV for detailed spectra. The beam diameter was roughly (6 × 7) mm^2. The non-monochromatic source was selected because it delivers higher energy relative to the monochromatic source and is thus more suitable in case elements in weak concentrations are to be determined. Among the possibilities of the XPS technique, attention was focused on the extraction of the oxidation states of elements from the treatment and recombining of complex photoelectric peaks. For palladium samples, a drop of the reaction mixture was deposited without any treatment on the silicon wafer and left to dry under an argon stream. Platinum samples were centrifuged at 5000 tpm for 20 min, redispersed in water, and washed two more times with water, centrifuged after each water addition, and finally redispersed in water. A drop of the solution is deposited on a silicon wafer and left to dry in a continuously argon-flushed box.

TEM observations: The TEM images were recorded on a JEOL 100CXII transmission electron microscope at an accelerating voltage of 100 kV. The sample drops were deposited and dried on carbon-coated copper grids.

Electrochemistry: The electrochemical experiments, the source, and mounting and polishing of the glassy carbon (GC Le Carbone Lorraine, France) electrodes has been described previously.[31] The electrochemical set-up was an EG&G 273 A driven by a PC with M270 software. Potentials are measured against a reference SCE. The counter electrode was a Pt gauze with a large surface area. Pure water from a RiOs 8 unit followed by a Millipore-Q Academic purification set was used throughout. The solutions were deaerated thoroughly for at least 30 min with pure argon and kept under a positive pressure during the experiments. The supporting electrolyte was a solution of 1 M LiCl + HCl at pH 2.

Acknowledgements

This study was supported by the CNRS (UMR 8180 and 8000), the Université de Versailles Saint-Quentin, the Université Paris-Sud 11, and the CEA-Saclay (Laboratoire de Réactivité des Surfaces et Interfaces). The help of Rosa N. Biboum during the preliminary experiments of nanoparticle synthesis is thankfully acknowledged. The authors thank Dr P. Beaunier (Université Paris VI) for the TEM analysis and Florence Ramiandrasoa (Université Paris XI) for the FTIR measurements.

[1] a) A. Proust, R. Thouvenot, P. Gouzerh, *Chem. Commun.* **2008**, 1837; b) P. Mialane, A. Dolbecq, F. Sécheresse, *Chem. Commun.* **2006**, 3477.
[2] a) B. Hasenknopf, R. Delmont, P. Herson, P. Gouzerh, *Eur. J. Inorg. Chem.* **2002**, 1081; b) P. R. Marcoux, B. Hasenknopf, J. Vaissermann, P. Gouzerh, *Eur. J. Inorg. Chem.* **2003**, 2406.
[3] A. Dolbecq, F. Sécheresse, *Adv. Inorg. Chem.* **2002**, *53*, 1.
[4] a) K. M. Barkigia, L. M. Rajkovic-Blazer, M. T. Pope, C. O. Quicksall, *Inorg. Chem.* **1981**, *20*, 3318; b) B. S. J. Johnson, R. C. Schroden, C. Zhu, A. Stein, *Inorg. Chem.* **2001**, *40*, 5972.
[5] a) U. Kortz, M. G. Savelieff, F. Y. Abou Gali, L. M. Khalil, S. A. Maalouf, D. I. Sinno, *Angew. Chem.* **2002**, *114*, 4246; *Angew. Chem. Int. Ed.* **2002**, *41*, 4070; b) U. Kortz, J. Vaissermann, R. Thouvenot, P. Gouzerh, *Inorg. Chem.* **2003**, *42*, 1135.
[6] U. Kortz, C. Marquer, R. Thouvenot, M. Nierlich, *Inorg. Chem.* **2003**, *42*, 1158.
[7] a) E. Cadot, F. Sécheresse, *Chem. Commun.* **2002**, 2189; b) J.-F. Lemonnier, S. Floquet, J. Marrot, E. Terazzi, C. Piguet, P. Lesot, A. Pinto, E. Cadot, *Chem. Eur. J.* **2007**, *13*, 3548.
[8] B. Modec, D. Dolenc, J. V. Brencic, J. Koller, J. Zubieta, *Eur. J. Inorg. Chem.* **2005**, 3224.
[9] a) C. du Peloux, A. Dolbecq, P. Mialane, J. Marrot, F. Sécheresse, *Dalton Trans.* **2004**, 1259; b) A. Dolbecq, L. Lisnard, P. Mialane, J. Marrot, M. Bénard, M.-M. Rohmer, F. Sécheresse, *Inorg. Chem.* **2006**, *45*, 5898.
[10] B. Keita, G. Zhang, A. Dolbecq, P. Mialane, F. Miserque, L. Nadjo, *J. Phys. Chem. A J. Phys. Chem. B* **2007**, *111*, 8145.
[11] G. Zhang, B. Keita, A. Dolbecq, P. Mialane, F. Sécheresse, F. Miserque, L. Nadjo, *Chem. Mater.* **2007**, *19*, 5821.
[12] N. E. Brese, M. O'Keeffe, *Acta Crystallogr. Sect. A* **1991**, *47*, 192.
[13] K. Y. Matsumoto, *Bull. Chem. Soc. Jpn.* **1979**, *52*, 3284.
[14] W. Kwak, L. M. RajkoviC J. K. Stalick, M. T. Pope, C. O. Quicksall, *Inorg. Chem.* **1976**, *15*, 2778.
[15] U. Kortz, G. B. Jameson, M. T. Pope, *J. Am. Chem. Soc.* **1994**, *116*, 2659.
[16] U. Kortz, M. T. Pope, *Inorg. Chem.* **1995**, *34*, 2160.
[17] H. Abbas, A. L. Pickering, D.-L. Long, P. Kögerler, L. Cronin, *Chem. Eur. J.* **2005**, *11*, 1071.
[18] C. Ritchie, E. M. Burkholder, D.-L. Long, D. Adam, P. Kögerler, L. Cronin, *Chem. Commun.* **2007**, 468.
[19] R. Contant, G. Hervé, *Rev. Inorg. Chem.* **2002**, *22*, 63.
[20] B. Keita, I.-M. Mbomekalle, L. Nadjo, C. Haut, *Electrochem. Commun.* **2004**, *6*, 978.
[21] B. Keita, L. Nadjo, D. Bélanger, C. P. Wilde, M. Hilaire, *J. Electroanal. Chem.* **1995**, *384*, 155.
[22] G. M. Maksimova, A. L. Chuvilin, E. M. Moroz, V. A. Likholobov, K. I. Matveev, *Kinet. Catal.* **2004**, *45*, 870.
[23] a) Y. Xia, P. Yang, Y. Sun, Y. Wu, M. Mayers, B. Gates, Y. Yin, F. Kim, H. Yan, *Adv. Mater.* **2003**,*15*, 353; b) B. Wiley, Y. Sun, B. Mayers, Y. Xia, *Chem. Eur. J.* **2005**, *11*, 454.
[24] G. Maayan, R. Neumann, *Chem. Commun.* **2005**, 4595.
[25] R. Narayanan, M. El Sayed, *Nano Lett.* **2004**, *4*, 1343.
[26] B. Keita, E. Abdeljalil, F. Girard, S. Gerschwiler, L. Nadjo, R. Contant, *J. Solid State Electrochem.* **1999**, *3*, 446.
[27] B. Keita, R. Contant, E. Abdeljalil, F. Girard, L. Nadjo, *Electrochem. Commun.* **2000**, *2*, 295.
[28] G. M. Sheldrick, SADABS, program for scaling and correction of area detector data, University of Göttingen Göttingen (Germany), **1997**.
[29] R. Blessing, *Acta Crystallogr. Sect. A* **1995**, *51*, 33.
[30] G. M. Sheldrick, SHELX-TL version 5.03, Software Package for the Crystal Structure Determination, Siemens Analytical X-ray Instrument Division, Madison, WI (USA), **1994**.
[31] B. Keita, L. Nadjo, *J. Electroanal. Chem.* **1988**, *243*, 87.

Received: April 15, 2008
Revised: October 13, 2008
Published online: November 28, 2008

